THE JOURNAL OF BIOLOGICAL CHEMISTRY VOL. 286, NO. 38, pp. 33501–33510, September 23, 2011

The Dystrophin-associated Protein Complex Maintains Muscle Excitability by Regulating Ca^{2+}-dependent K^+ (BK) Channel Localization*[S]

Received for publication, February 2, 2011, and in revised form, July 7, 2011 Published, JBC Papers in Press, July 27, 2011, DOI 10.1074/jbc.M111.227678

Feyza Sancar[‡1], Denis Touroutine[§1], Shangbang Gao[¶1], Hyun J. Oh[‖], Marie Gendrel[**], Jean-Louis Bessereau[‡‡§§], Hongkyun Kim[‖], Mei Zhen[¶], and Janet E. Richmond[‡2]**

*From the [‡]Department of Biological Sciences, University of Illinois-Chicago, Chicago, Illinois 60607, the [§]Department of Neurobiology, University of Massachusetts Medical School, Worcester, Massachusetts 01605, the [¶]Samuel Lunenfeld Research Institute, University of Toronto, Toronto, Ontario M5G 1X5, Canada, the [‖]Department of Cell Biology and Anatomy, Rosalind Franklin University of Science and Medicine, North Chicago, Illinois 60064, the **Biology Department, Institut de Biologie de l'Ecole Normale Superieure, F-75005 Paris, France, the [‡‡]Inserm, Unite 1024, F-75005 Paris, France, and the [§§]Centre National de la Recherche Scientifique, Unit e Mixte de Recherche 8197, F-75005 Paris, France*

The dystrophin-associated protein complex (DAPC) consists of several transmembrane and intracellular scaffolding elements that have been implicated in maintaining the structure and morphology of the vertebrate neuromuscular junction (NMJ). Genetic linkage analysis has identified loss-of-function mutations in DAPC genes that give rise to degenerative muscular dystrophies. Although much is known about the involvement of the DAPC in maintaining muscle integrity, less is known about the precise contribution of the DAPC in cell signaling events. To better characterize the functional role of the DAPC at the NMJ, we used electrophysiology, immunohistochemistry, and fluorescent labeling to directly assess cholinergic synaptic transmission, ion channel localization, and muscle excitability in loss-of-function (lf) mutants of *Caenorhabditis elegans* DAPC homologues. We found that all DAPC mutants consistently display mislocalization of the Ca^{2+}-gated K^+ channel, SLO-1, in muscle cells, while ionotropic acetylcholine receptor (AChR) expression and localization at the NMJ remained unaltered. Synaptic cholinergic signaling was also not significantly impacted across DAPC(lf) mutants. Consistent with these findings and the postsynaptic mislocalization of SLO-1, we observed an increase in muscle excitability downstream of cholinergic signaling. Based on our results, we conclude that the DAPC is not involved in regulating AChR architecture at the NMJ, but rather functions to control muscle excitability, in an activity-dependent manner, through the proper localization of SLO-1 channels.

The dystrophin-associated protein complex (DAPC)[3] has been implicated in the structural maturation and maintenance of the muscle sarcolemma and neuromuscular junction (NMJ) in vertebrates (1, 2). The DAPC is composed of the plasma membrane spanning dystroglycans and sarcoglycans, of which α-dystroglycans bind directly to extracellular matrix proteins. The cytoplasmic DAPC components consist of dystrobrevin, syntrophin, and dystrophin, of which dystrophins bind directly to the cytoskeletal protein F-actin. Loss-of-function (lf) mutations in DAPC sarcoglycans and dystrophin are known to cause the heritable degenerative muscular dystrophies, Limb-Girdle and Duchenne/Becker, respectively, in humans (3). Prevailing scientific evidence posits that the DAPC maintains membrane stability during muscle contraction by linking the cytoskeleton to extracellular matrix proteins such as Laminin and Perlecan (see Refs. 2, 4 for reviews). Therefore, in the absence of the DAPC, uncoupling of the extracellular matrix from the muscle cytoskeleton results in cytoskeletal instability that ultimately causes muscle membrane rupture and subsequent necrosis during contractile activity (5). However, more recent evidence suggests that in addition to their role in maintaining muscle integrity, the DAPC may actively participate in signal transduction events, as the DAPC associates with signaling molecules such as nNOS, calmodulin, CaMKII, and protein kinase A (PKA) (see Ref. 6 for review). Furthermore, dystrophin has been implicated in aggregating, clustering and/or maintaining AChRs at the NMJ (7). It has been postulated that the loss of dystrophin at the NMJ may, by disrupting receptor aggregation, alters the properties of AChRs making them more permeable to Ca^{2+} thus leading to Ca^{2+}-induced cellular toxicity (5). Although dystrobrevin, dystroglycan, and syntrophin have also been shown to play an important role in the maintenance and stabilization of AChR clusters at the vertebrate NMJ (8–10), mutations in these DAPC genes have not yet been linked to human muscular dystrophy syndromes despite the fact that genetic deletions of dystroglycan and dystrobrevin in mice recapitulate many of the degenerative muscular changes that occur in humans (3, 9, 11).

The nematode *Caenorhabditis elegans* has proven to be a powerful model system for investigation of neuromuscular

* This study was supported, in whole or in part, by National Institutes of Health Grants R01 MH073156 (to J. E. R.), and R01 NS058814 (to H. K.); the Canadian Institute Health Research Grants (MOP-93619 and MOP-74530) (to M. Z.); and INSERM, the Fondation pour la Recherche Medicale and the Association Française contre les Myopathies (to J.-L. B.).

[S] The on-line version of this article (available at http://www.jbc.org) contains supplemental Fig. S1.

[1] These authors contributed equally to this work.

[2] To whom correspondence should be addressed: Dept. of Biological Sciences, University of Illinois-Chicago, 840 W. Taylor St., Chicago, IL 60607. Tel.: 312-413-2513; E-mail: jer@uic.edu.

[3] The abbreviations used are: DAPC, dystrophin-associated protein complex; NMJ, neuromuscular junction; AChR, ionotropic acetylcholine receptor; N-AChR, nicotine sensitive ACR-16 acetylcholine receptors; L-AChR, levamisole sensitive acetylcholine receptors.

development and function, as NMJ physiology and morphology can be addressed with relative ease using genetic, transgenic, electrophysiolgical, pharmacological, and optical imaging approaches. Genetic dissection of *C. elegans* has confirmed the conservation of DAPC components dystroglycan (*dgn-1*), dystrophin (*dys-1*), dystrobrevin (*dyb-1*), syntrophin (*stn-1*), δ/γ-sarcoglycan (*sgn-1*), and the C-terminal PDZ-domain ligand of nNOS (CAPON; *dyc-1*), most of which (with the exception of DGN-1) are expressed in *C. elegans* muscle cells. Furthermore, *in vitro* biochemical and genetic analyses have demonstrated putative physical and functional interactions between *C. elegans* DAPC homologues, providing further evidence that *C. elegans* assembles a DAPC comparable and analogous to that of vertebrates and can thus provide insights into the role of the DAPC in mammalian NMJ function and pathology (12–15). Importantly, previous studies reported that null mutations in *C. elegans* DAPC genes result in common movement defects consistent with muscle hyperexcitability and enhanced cholinergic transmission (13–19). However, there has been no systematic electrophysiological characterization of *C. elegans* DAPC mutants, therefore it remains to be seen whether these mutants directly regulate cholinergic release, AChR function, or downstream muscle excitability. In line with the involvement of DAPC proteins in cell signaling events, a subset of the DAPC genes (*dys-1* and *stn-1*) have recently been implicated in the proper targeting/function of the Ca^{2+}-dependent K^+ channel (BK channel) SLO-1 in muscle cells (20).

In this study, we attempt to identify a unifying cellular mechanism that could account for the reported phenotypic similarities across *C. elegans* DAPC mutants. We used *in situ* whole-cell patch-clamp electrophysiology, immunohistochemical staining, and fluorescently tagged reporter constructs to directly assess cholinergic synaptic transmission, AChR and SLO-1 localization, and muscle excitability in DAPC mutants. Our results indicate that DAPC mutants cause activity-dependent muscle hyperexcitability downstream of cholinergic signaling, due to altered SLO-1 localization.

EXPERIMENTAL PROCEDURES

Strains and Culturing Conditions

The genotypes of animals used in this study were are follows: the wild-type Bristol isolate N2; DAPC loss-of-function (lf) alleles *dys-1(cx18)*, *dyb-1(cx36)*, *dyc-1(cx32)*, *stn-1(ok292)*, *slo-1(js379)* obtained from the CGC; the transgenic channelrhodopsin line *zxIs6*[*punc-17::chop-2(H134R)::yfp;lin-15*+] (21); and the fluorescent reporter line *cimIs1*[*slo-1a::GFP; rol-6(d)*] (20). The body-wall muscle expressed ACR-16::GFP reporter line, *jaSi4*[*Pmyo-3:acr-16::gfp*], was generated using the Mos-1-mediated single copy insertion (MOSCI) technique (22) and crossed into the *acr-16(ok789)*-null background. *zxIs6*, *cimIs1, and jaSi4;acr-16(ok789)* lines were crossed into DAPC(lf) mutant backgrounds for subsequent electrophysiological or confocal microscopy analysis. All strains used were outcrossed at least twice. Animals were cultured at 15–22 °C on OP50-seeded NGM plates. For electrophysiological recordings, *zxIs6* and *zxIs6;DAPC(lf)* doubles were cultured in the dark at 15–22 °C on OP50-seeded NGM plates supplemented with all-*trans* retinal as described previously (21).

Microscopy

For analysis of SLO-1::GFP expression, animals were imaged as described (23). In brief, fluorescence images were obtained using a Zeiss Axio Observer microscope with a 40× objective (water-immersion, NA:1.2) or an Olympus Fluoview 300 confocal microscope with a 60× objective (oil-immersion, NA:1.4) or 100× objective (oil-immersion, NA:1.4). Over 50 animals were analyzed for each genotype. Images for fluorescence quantification were acquired under identical exposure time, gain, and pin-hole diameter. The intensity of fluorescent SLO-1::GFP puncta from confocal images was analyzed using linescan (Metamorph, Molecular Devices) and presented as values obtained by subtracting background levels from averaged peak gray levels of puncta. For analysis of ACR-16::GFP expression, fluorescence images were obtained using an Olympus Fluoview™ laser-scanning confocal microscope with 40× objective (oil-immersion) and reconstructed/merged using the image-processing program ImageJ. All images were acquired under identical laser-scanning settings, with at least 4 animals imaged per genotype. Immunofluorescence staining for UNC-38 was examined under the Confocal Leica TCS SP5 microscope. Image reconstruction and merges were obtained with ImageJ. For the sake of consistency, representative confocal images of UNC-38 and ACR-16 localization in Fig. 2 were of dorsal nerve cord sections, as immumohistochemical labeling of UNC-38 was more consistent and reliable at the dorsal nerve cord relative to the ventral nerve cord.

Immunostaining

Antibodies against UNC-38 were produced as previously described (24). Worms were prepared using the freeze-crack method (25). In brief, animals were freeze-cracked using SuperFrost Plus slides (Menzel-Glaser) and fixed in −20 °C methanol for 5 min and in −20 °C acetone for 5 min. Worms were then collected in 1× PBS and immunofluorescence staining was performed on fixed worms in suspension. Samples were blocked for 30 min at room temperature with 0.2% fish gelatin (Sigma). Anti-UNC-38 antibodies were used at a 1:800 dilution. Preparations were incubated with the following secondary antibody for 3 h at room temperature: Cy3-labeled goat anti-rabbit IgG (H+L) (Jackson ImmunoResearch Laboratories) at a dilution of 1:1,000.

Immunoblotting

Western blot analysis was performed as previously described (23). Briefly, mixed staged worms were washed and collected in M9 buffer. Equal volumes of 2× Laemmli sample buffer was added to the worm pellets. The resulting worm suspension was heated at 90 °C for 10 min, centrifuged at 20,000 × *g* for 10 min. and then loaded on 7.5% SDS-PAGE gel immediately. For protein detection, an anti-GFP antibody (Clontech, JL-8), anti-α-tubulin antibody (Developmental hybridoma bank, AA4.3) and an HRP-conjugated goat anti-mouse IgG (Millipore) were used.

Electrophysiology

Voltage-clamp Recordings—Voltage-clamp recordings were performed as previously described (26). Briefly, animals were

raised on NGM plates seeded with OP50 bacteria containing 80 μM retinal. Prior to analysis, adult hermaphrodites were immobilized with cyanoacrylic glue and the ventral medial body wall muscles exposed by lateral cuticle excisions. Body-wall muscle cell recordings were made in the whole-cell voltage-clamp configuration (holding potential of −60 mV) using an EPC-10 patch-clamp amplifier and digitized at 2.9 Hz. The extracellular solution consisted of (in mM): NaCl 150; KCl 5; $CaCl_2$ 5; $MgCl_2$ 4; glucose10; sucrose 5; HEPES 15 (pH 7.3, ~340mOsm). The patch pipette (fire-polished 4–6 MOhm resistant borosilicate pipettes; World Precision Instruments) was filled with (in mM): KCl 120; KOH 20; $MgCl_2$ 4; (*N*-Tris[Hydroxymethyl]methyl-2-aminoethane-sulfonic acid) 5; $CaCl_2$ 0.25; Na_2ATP 4; sucrose 36; EGTA 5 (pH 7.2, ~315 mOsm). All animals contained the transgene *ZxIs6* expressing channelrhodopsin-2 under the control of the cholinergic motor neuron-specific promoter (*Punc-17*). Photoevoked currents were recorded in body-wall muscle cells after a 10 ms illumination using a 470 nm LED (Thor Labs) triggered with a TTL pulse from the EPC10 pulse generator (21). Evoked post-synaptic responses were acquired using Pulse software (HEKA) run on a Dell computer. Subsequent analysis and graphing of evoked responses was performed using Pulsefit (HEKA) and Igor Pro (Wavemetrics). At least five independent measurements were obtained per genotype, and statistical analyses were determined by one-way ANOVA followed by a post hoc Dunnett's test of significance (Prism, GraphPad Software Inc., San Diego, CA).

Current Clamp Recordings—Current-clamp recordings were performed as previously described (27). Briefly, animals were dissected as detailed above. Body wall muscle cell recordings were made in the whole-cell current-clamp configuration by a Digidata 1440A and MultiClamp 700A amplifier, using the Clampex 10 software and processed with Clampfit 10 (Axon Instruments, Molecular Devices). Data were digitized at 10–20 kHz and filtered at 2.6 kHz. Cell resistance and capacitance were determined with Clampex by applying a 10 mV depolarizing pulse with a holding potential of −60 mV. For recording resting membrane potential and action potentials, the extracellular solution was prepared as for voltage-clamp recording, with the exception that the $MgCl_2$ concentration was 1 mM. The patch pipette (fire-polished 4–6 MOhm resistant borosilicate pipettes; World Precision Instruments) was filled (in mM) with: K-gluconate 115; KCl 25; $CaCl_2$ 0.1; $MgCl_2$ 5; BAPTA 1; HEPES 10; Na_2ATP 5; Na_2GTP 0.5; cAMP 0.5; cGMP 0.5 (pH7.2 with KOH, ~320 mOsm). For action potential recordings, light stimulation of *zxIs6* was performed using an LED lamp (KSL-70, RAPP OptoElectronic, Germany), at a wavelength of 490 nm (8 milliwatt/mm^2) controlled by the Axon amplifier software. At least 7 independent measurements were obtained per genotype, and statistical differences were determined by one-way ANOVA followed by a post hoc Dunnett's test of significance (Prism, GraphPad Software Inc.).

RESULTS

Loss-of-Function Mutations in DAPC Genes Do Not Impact NMJ Cholinergic Response Amplitudes—DAPC(lf) mutants exhibit a characteristic behavioral phenotype consisting of exaggerated head-bending and muscular hypercontraction, associated in some mutants with increased sensitivity to the acetylcholinesterase inhibitor aldicarb (13, 16–19). These characteristics suggest that cholinergic signaling may be enhanced in DAPC mutants. Enhanced cholinergic signaling in DAPC(lf) mutants could arise through changes in presynaptic ACh release, or altered postsynaptic function in either or both of the two muscle acetylcholine receptor types (AChRs); one of which is the levamisole-sensitive AChR (L-AChR) composed of essential subunits UNC-29, UNC-38, and UNC-63, and the second is the nicotine-sensitive ACR-16 AChR (N-AChR), named for the identity of its essential receptor subunit encoded by *acr-16*. Interestingly, SLO-1(lf) mutants closely phenocopy DAPC(lf) mutants and display enhanced quantal neurotransmitter release (28). However, the role of SLO-1, if any, in AChR architecture remains to be elucidated. We hypothesize that SLO-1(lf) and DAPC(lf) mutants, given their phenotypic similarities, may all share a common defect in synaptic neurotransmission as a reflection of enhanced cholinergic signaling.

To examine cholinergic synaptic responses in SLO-1(lf) [*slo-1(js379)*] and DAPC(lf) mutants [*dys-1(cx18)*, *dyb-1(cx36)*, *dyc-1(cx32)*, and *stn-1(ok292)*] we recorded evoked NMJ currents from voltage-clamped body wall muscles of respective mutant reference alleles in response to blue-light activated ACh release from cholinergic ventral cord motor neurons expressing channelrhodopsin (21, 29). The peak evoked response (Fig. 1*A*) is predominantly mediated by N-AChRs, as the L-AChR accounting for less than 20% of the maximal evoked response is slow to activate (Fig. 1*C*) (30). The ACR-16-mediated current response amplitudes from body wall muscle cells in DAPC reference alleles were similar to wild-type (WT), ranging from ~1.5–2 nA (Fig. 1, *A* and *B*). L-AChR-mediated photoevoked responses were then isolated by blocking ACR-16 nAChR responses with the ACR-16 nAChR-selective antagonist DHβE (Fig. 1, *C* and *D*). The remaining L-AChR-mediated photoevoked responses were also unaltered in DAPC reference alleles, ranging from ~300–450 pA (Fig. 1, *C* and *D*).

Although we did not observe any differences in the NMJ evoked response amplitudes of SLO-1(lf) and DAPC(lf) mutants, we did observe kinetic changes in photoevoked current responses (Fig. 1, *E* and *F*). Specifically, *slo-1(js379)* and *stn-1(ok292)* displayed a ~2-fold increase in the half-time decay of photoevoked currents relative to WT ($t_{1/2}$ values for *slo-1(js379)* = 13.6 ± 1.4 ms; *stn-1(ok292)* = 12.8 ± 1.1 ms; WT = 6.4 ± 0.8 ms; both $p < 0.01$)(Fig. 1*F*). Because STN-1 is reported to stabilize and maintain SNF-6 (an acetylcholine uptake transporter) at the postsynaptic muscle membrane (31), we attributed the slowed decay of evoked responses in *stn-1(ok292)* mutants to an accumulation of ACh at the synapse, similar to that previously observed in *snf-6* mutants. As SLO-1 negatively regulates presynaptic neurotransmitter release at the *C. elegans* NMJ (28), the slowed decay of current responses in *slo-1(js379)* likely reflects loss of presynaptic SLO-1 function and consequent enhanced presynaptic acetylcholine release. However, the prolonged decay of photoevoked current responses was not an electrophysiological phenotype common to all DAPC reference alleles (Fig. 1, *E* and *F*), suggesting that alterations in cholinergic muscle response kinetics alone can-

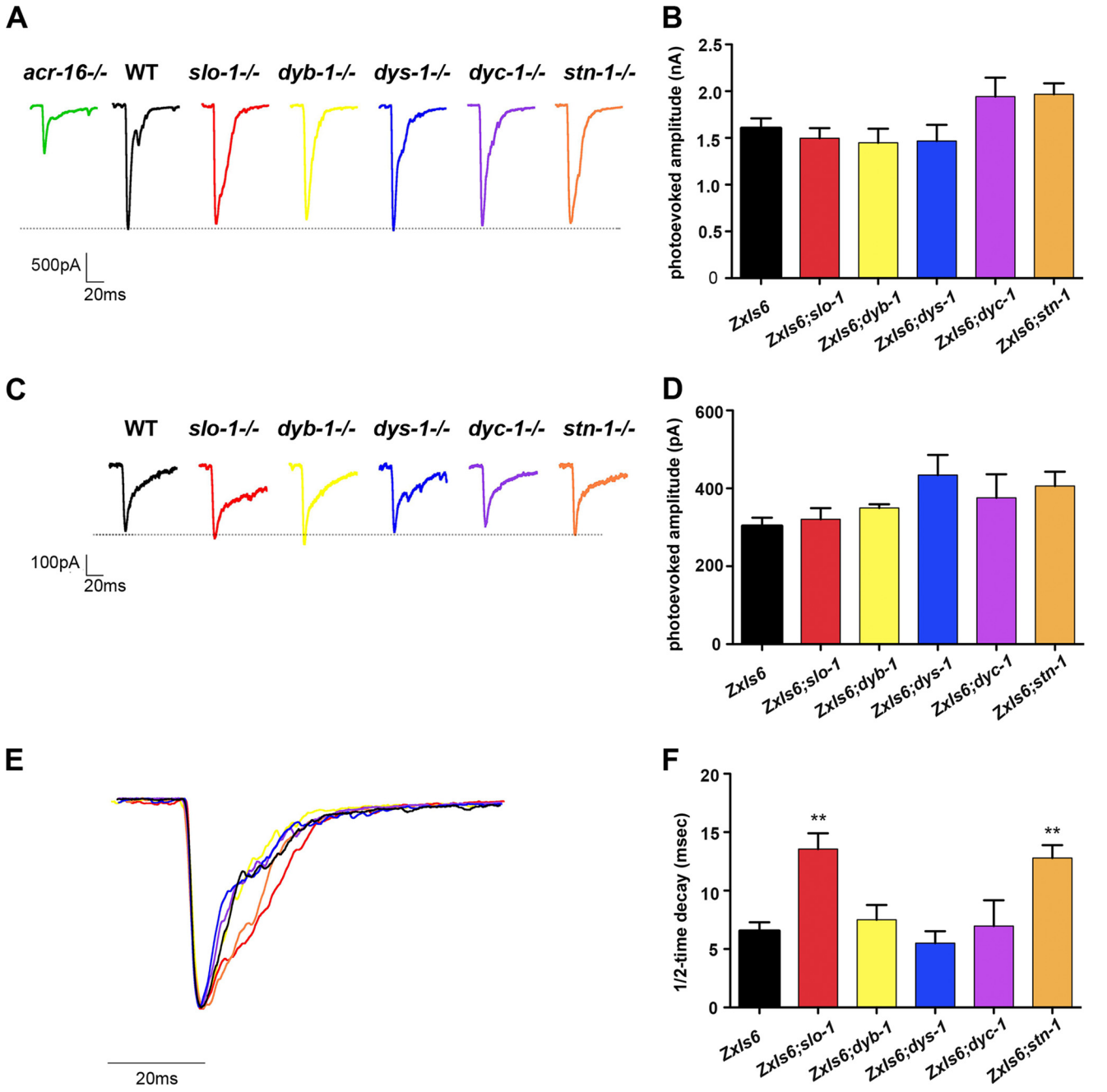

FIGURE 1. **Optogenetic analysis of cholinergic signaling at the NMJ in DAPC(lf) mutants.** *A*, representative traces of synaptic currents elicited in voltage-clamped ventral body wall muscle cells by 10 ms blue-light photostimulation of the ventral nerve cord at the NMJ of WT, SLO-1(lf), and DAPC(lf) alleles (colors correspond to genotypes in *B*). If N-AChR function is altered, we would anticipate a significant reduction in the maximal synaptic response amplitude relative to WT, as observed with ACR-16(lf) (*green trace*). *B*, averaged photoevoked muscle response amplitudes in SLO-1(lf) and DAPC(lf) alleles are similar to WT (mean ± S.E.; $n \geq 5$ per genotype). *C*, representative traces of photoevoked currents elicited in voltage-clamped body-wall muscles bathed in DHβE, isolating the L-AChR component of the synaptic response (colors correspond to genotypes in *D*). *D*, averaged photoevoked muscle response amplitudes mediated by Lev-nAChRs are similar across SLO-1(lf) and DAPC(lf) alleles relative to WT (mean ± S.E.; n≥3 per genotype). *E*, representative normalized superimposed traces of photoevoked synaptic current responses in muscles reveals kinetic differences in the synaptic response across SLO-1(lf) and DAPC(lf) mutants relative to WT (colors correspond to genotypes in *F*). *F*, averaged $^1/_2$-time decay of photoevoked currents are significantly slowed only in *stn-1(lf)* and *slo-1(lf)* alleles relative to WT (**, $p < 0.01$; mean ± S.E.; $n \geq 5$ per genotype). Statistical significance was determined using a one-way ANOVA with Dunnett's post-test.

not account for the mechanism underlying the phenotypic similarities across SLO-1(lf) and DAPC(lf) mutants.

Expression and Localization of AChRs Are Unaffected at the NMJ in DAPC(lf) Mutants—Normal amplitudes for both AChR components of the NMJ photoevoked response in SLO-1 and DAPC mutants suggest that the number of cholinergic AChRs expressed in muscle cells is unaffected by a loss of SLO-1 or the DAPC. To directly assess AChR expression and synaptic localization in SLO-1 and DAPC reference alleles, we immunostained for the L-AChR subunit, UNC-38, in freeze-cracked WT and DAPC mutant animals using antibodies raised against UNC-38 (24). To assess postsynaptic muscle ACR-16 expression, we generated an integrated ACR-16::GFP reporter line using the Mos-1-mediated single copy insertion (MOSCI) tech-

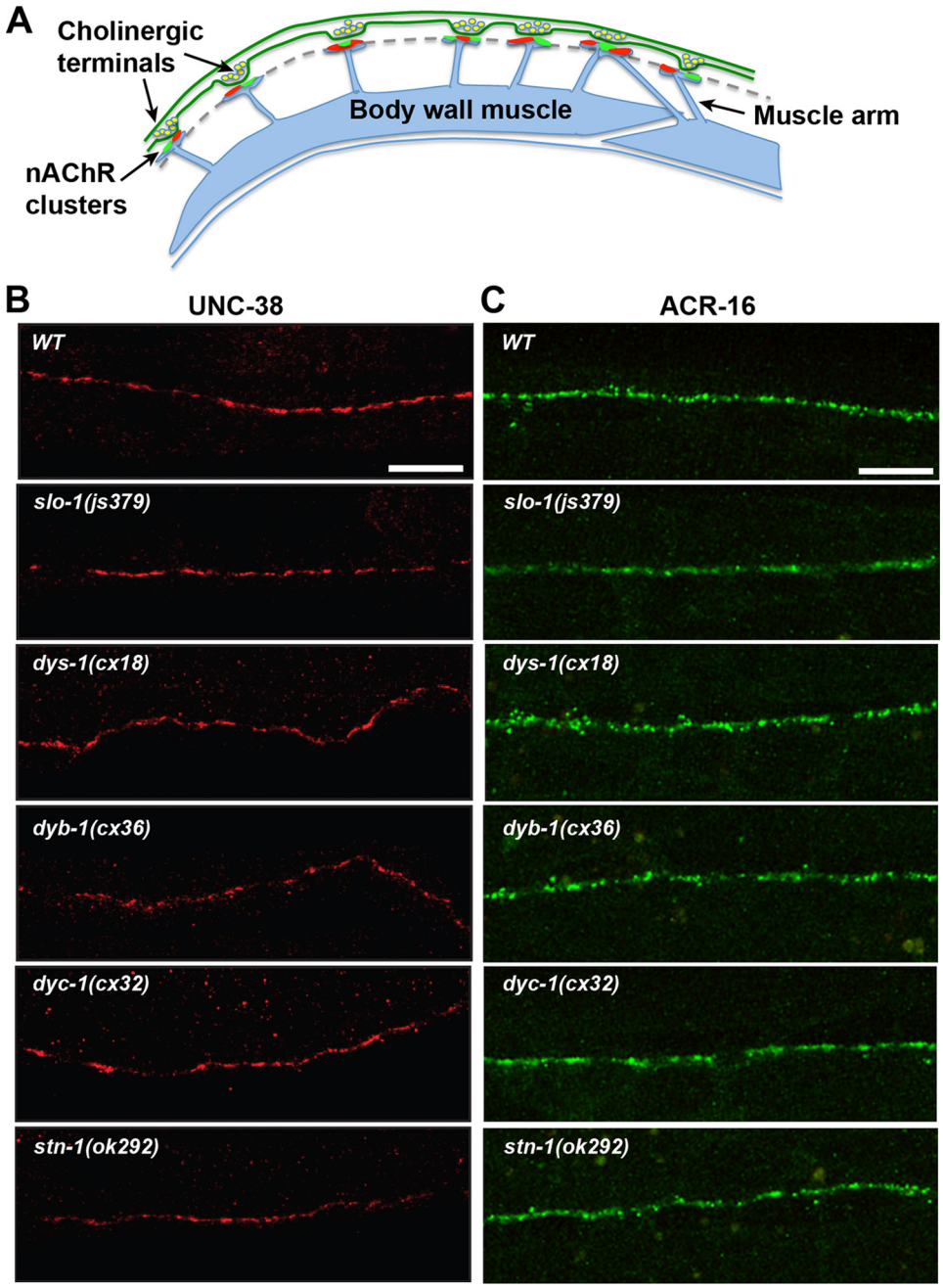

FIGURE 2. **Immunostaining and confocal fluorescence analysis of ACR-16 and UNC-38 AChR expression in muscle cells at the NMJ of DAPC(lf) reference alleles.** *A*, schematic representation of the *C. elegans* dorsal nerve cord NMJ organization. Puncta representing post-synaptic clusters of UNC-38 containing L-AChRs (*red*) and ACR-16 containing nAChRs (*green*) occur adjacent to cholinergic presynaptic terminals along the nerve cord, as indicated by the *dashed line*. *B*, representative antibody staining for UNC-38 in DAPC(lf) alleles reveals discrete UNC-38 clustering along the nerve cord, similar to WT. Scale, 10 μm. *C*, representative confocal projection images of post-synaptic muscle ACR-16::GFP expression in DAPC(lf) alleles reveals discrete ACR-16 clustering along the nerve cord, similar to WT. Scale, 10 μm. The ACR-16::GFP construct and ACR-16::GFP;DAPC(lf) doubles were generated and analyzed in the *acr-16(ok789)* background as described under "Experimental Procedures."

nique, where expression was driven by the *myo-3* body-wall-muscle specific promoter (*jaSi4*[*Pmyo-3:acr-16::gfp*]) (22). The *jaSi4* MOSCI transgenic and *jaSi4*;DAPC(lf) lines were analyzed in an ACR-16-null background (*acr16(ok789)*) to eliminate contribution of endogenous untagged ACR-16 and better recapitulate endogenous muscle expression levels (Fig. 2*B*). At wild type NMJs, both nicotinic receptor types cluster as postsynaptic puncta at the tips of muscles arms that extend to the nerve cord and contact *en passant* presynaptic terminals (Fig. 2*A*, and further histological details at http://www.wormatlas.org/hermaphrodite/muscleintro/mainframe.htm). In all DAPC mutant backgrounds, UNC-38 and ACR-16 were clustered along the nerve cord, similar to WT (Fig. 2, *B* and *C*, respectively). Taken together, analysis of cholinergic current response amplitudes and AChR expression at the NMJ suggests that the DAPC does not directly regulate AChR function or localization.

The DAPC Is Necessary for Localization of SLO-1 in Body Wall Muscle Cells, but Not in Neurons—Previous work has shown that *dys-1* mutants exhibit mislocalization of SLO-1 in

body wall muscle cells, and indirect evidence suggests the DAPC regulates SLO-1 expression via the SLO-1 interacting protein ISLO-1 (20). In an effort to determine whether all DAPC proteins share a common cellular function in the regulation of SLO-1, we assessed the localization and distribution of SLO-1 in DAPC(lf) mutants using an integrated SLO-1::GFP translational fusion reporter line (*cimIs1*[*slo-1a::GFP,rol-6(d)*]) (20). In wild-type animals, SLO-1::GFP is expressed in the muscle membrane in a punctate pattern closely resembling that of dense body localization (Fig. 3) (20). We observed a marked reduction of ~75–90% in the intensity of SLO-1::GFP puncta in muscle cells across all DAPC(lf) mutants relative to WT ($p < 0.001$; Fig. 3, *A* and *B*), thereby identifying a common underlying defect in SLO-1 localization resulting from DAPC loss-of-function.

To confirm that the decrease in SLO-1::GFP intensity in DAPC(lf) muscles is a consequence of mislocalization rather than reduced expression, we assessed the levels of SLO-1::GFP protein in WT and DAPC(lf) lines. Western blot analysis reveals no difference in total SLO-1::GFP protein between WT and DAPC(lf) mutants (Fig. 3*E*), which suggests that the DAPC mediates localization and not expression of SLO-1. Interestingly, we did not observe a similar reduction of SLO-1:GFP signal intensity in ventral or dorsal cord neurons of DAPC(lf) mutants (Fig. 3, *C* and *D*), indicating that the DAPC selectively regulates muscle SLO-1 localization.

Loss of SLO-1 Function in Body Wall Muscles of DAPC Mutants Alters Muscle Excitability by Enhancing Stimulated Action Potential Bursts—Previous electrophysiological studies of the *C. elegans* NMJ have established that body wall muscle cells generate typical action potentials triggered by cholinergic synaptic transmission (27, 32). To ascertain whether SLO-1 mislocalization or down-regulation affects muscle excitability in DAPC mutants, we first measured the resting membrane potential of SLO-1(lf) and DAPC(lf) mutants under current-clamp conditions as described previously (27). The mislocalization of SLO-1 in muscle cells of DAPC mutants did not alter resting muscle membrane potential (Fig. 4*D*), suggesting that SLO-1 channels are not necessary or responsible for maintaining resting muscle tone. However, when we measured muscle AP bursts following 10 ms photo-stimulation of cholinergic motor neurons, the number of APs was significantly enhanced across SLO-1(lf) and DAPC(lf) mutants relative to WT (Fig. 4, *A–C* and see supplemental Fig. S1 for temporal representations of all AP data). Specifically, WT muscle generated ~3–4 photoevoked APs, while SLO-1(lf) and DAPC(lf) mutant muscles generated a 2-fold increase in photoevoked APs (*, $p < 0.05$ and **, $p < 0.01$; Fig. 4*C*). The observed augmentation of AP number appeared to be specific to photoevoked action potentials, as the frequency of spontaneous APs (at a 0pA holding current) was reported to be unchanged in SLO-1(lf) mutants (27). These findings suggest that SLO-1 is necessary to repolarize the muscle membrane after prolonged periods of presynaptic neuronal activity, and without proper SLO-1-mediated repolarization of the membrane, the muscle cells exhibit persistent iterative action potentials. These results provide evidence that the loss of SLO-1 function in DAPC mutants enhances muscle excitability in an activity-dependent manner.

DISCUSSION

DAPC Proteins Are Required for Proper Localization of SLO-1 in Muscle Cells—In this study, we demonstrated that components of the DAPC complex are individually required for proper localization of SLO-1 in *C. elegans* body wall muscle cells. These findings are in agreement with previous studies that implicate *dys-1* and *stn-1* (via the adaptor protein ISLO-1) in localizing or binding SLO-1 (20). We assert that the DAPC tethers SLO-1 channels to muscle dense bodies, as is demonstrated by the lack of discrete SLO-1::GFP puncta at dense bodies in DAPC(lf) mutants. The DAPC likely maintains and stabilizes SLO-1 localization through physical interactions between STN-1/ISLO-1/SLO-1 (20). That SLO-1 protein levels are unaltered in DAPC mutants (Fig. 3*E*) further supports our proposed mechanism in which the DAPC anchors SLO-1 in the muscle membrane, rather than regulating SLO-1 expression.

It has long been recognized that DAPC mutants display strikingly similar behavioral phenotypes, characterized by hyperactivity and exaggerated curvature of the anterior body shape (referred to as "head-bending"). However, the underlying mechanism responsible for the near identical DAPC mutant phenotypes has remained elusive. Our findings are the first to identify a common cellular defect across DAPC mutants, the mislocalization of SLO-1 in body wall muscles, which can account for their phenotypic similarity. That DAPC mutant phenotypes are non-additive, *i.e.* single and double mutants display similar behavioral defects, further support our conclusion that DAPC proteins share in a common functional or signaling pathway (13, 19).

DAPC Regulates Muscle Excitability via SLO-1—In an effort to identify the underlying physiological function of the DAPC, we characterized synaptic properties of cholinergic NMJs across the family of DAPC mutants. To our knowledge, our results are the first to directly compare and systematically analyze synaptic neurotransmission in DAPC mutants. Based on our electrophysiological findings, the mislocalization of SLO-1 in DAPC mutants correlates with a common physiological profile of enhanced muscle excitability following presynaptic muscle stimulation, which is also shared by SLO-1(lf) mutants. It is unlikely that the alteration in muscle activity is due to changes in residually expressed SLO-1 function at the single channel level, as *in situ* patch-clamp recordings from body-wall muscle cells demonstrate that SLO-1 channel properties in *dys-1* mutants resemble WT (14). Given the role of SLO-1 as a Ca^{2+}-activated K^+ channel, the down-regulation of SLO-1 in muscle likely impairs rapid and robust repolarization of the membrane, thereby disinhibiting action potential generation. Current-clamp experiments in *C. elegans* have previously shown that increased action potential firing in body-wall muscle coincides with enhanced muscle contractility (27). As such, the measurable increase in intrinsic muscle excitability can mechanistically account for the hypercontraction reported for DAPC mutants. It is also in line with the ACh dose-dependent enhancement of pharyngeal muscle depolarization in *dys-1* and *dyb-1* mutants relative to WT (17, 19). Taken together, these findings imply that the DAPC negatively regulates, or controls, muscle excitability and contractility by insuring robust mem-

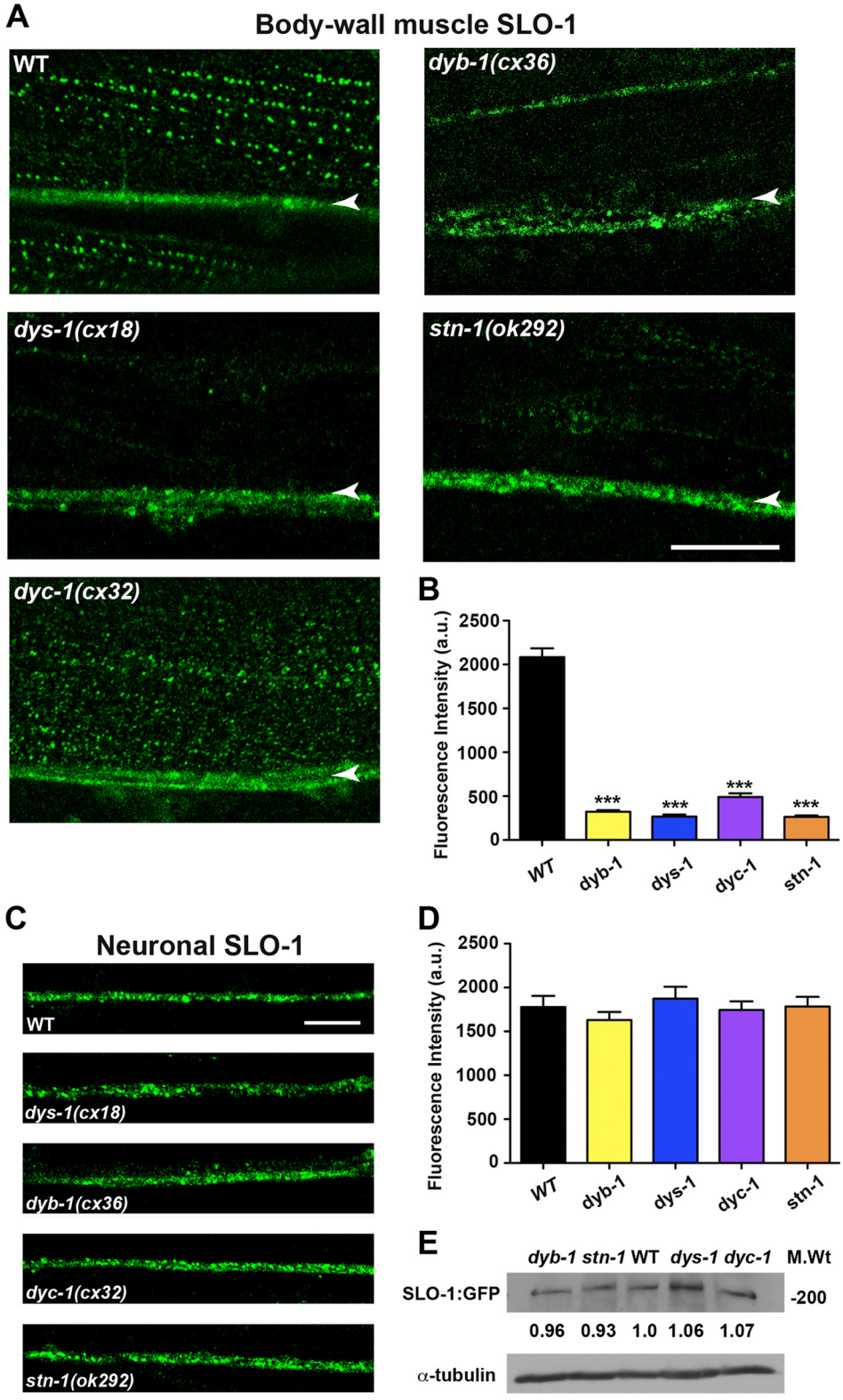

FIGURE 3. **Confocal analysis of SLO-1:GFP expression in muscle cells and neurons of DAPC(lf) mutants.** *A*, representative confocal images of SLO-1::GFP localization in DAPC(lf) mutants. SLO-1::GFP is expressed in punctate linear arrays that correspond to the localization of dense bodies. The *arrowheads* mark SLO-1::GFP localization at the nerve cord. Scale, 10 μm. *B*, averaged fluorescent intensity of SLO-1::GFP puncta in muscle cells is significantly reduced in DAPC(lf) mutants relative to WT (***, $p < 0.001$; mean $\pm$ S.E.; $n \geq 50$ per genotype). Statistical significance was determined using a one-way ANOVA with Dunnett's post-test. *C*, representative confocal images of neuronal SLO-1::GFP localization in DAPC reference alleles. Scale, 10 μm. *D*, averaged fluorescent intensity of SLO-1::GFP puncta in neurons of DAPC(lf) reference alleles is similar to WT (mean $\pm$ S.E.; n $\geq$ 50 per genotype), suggesting the DAPC does not regulate neuronal SLO-1 localization. *E*, SLO-1::GFP expression levels in wild-type and DAPC(lf) mutants.Western blot analysis reveals that the expression of SLO-1::GFP protein (as detected by an anti-GFP antibody, α-GFP) was not altered in DAPC(lf) mutants, relative to wild-type (*WT*) (*upper panel*). Loading controls (*lower panel*) reveal equivalent protein levels for tubulin (as detected by an anti-tubulin antibody, α-tubulin). The quantification was performed with Image J. Three independent experiments showed similar results.

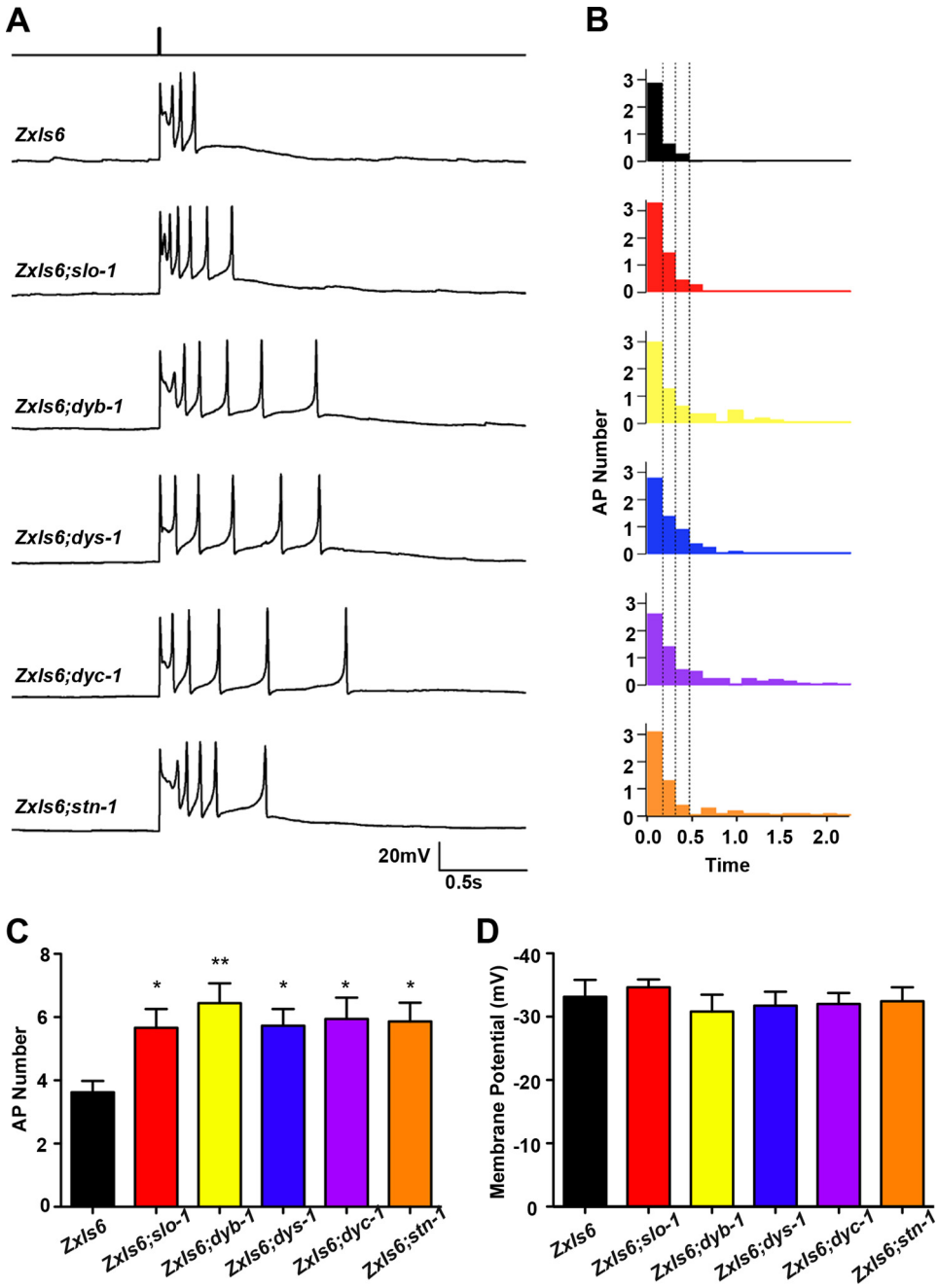

FIGURE 4. **Current clamp analysis of DAPC(lf) reference alleles in body wall muscles.** *A*, representative photoevoked action potential (*AP*) responses from current-clamped muscle cells at the NMJ of SLO-1(lf) and DAPC(lf) mutant alleles. The top step-trace represents the temporal location of the 10 ms blue-light stimulation. *B*, plots of average number of muscle APs as a function of time following photostimulation reveal a greater number of APs at later time points in SLO-1(lf) and DAPC(lf) mutants relative to WT. *C*, average number of muscle APs observed over a period of ~2.1 s following photostimulation is significantly greater in SLO-1(lf) and DAPC(lf) alleles relative to WT (*, $p < 0.05$; **, $p < 0.01$; mean ± S.E.; $n \geq 7$ per genotype), suggesting enhanced muscle excitability in SLO- 1(lf) and DAPC(lf) mutants. Statistical significance was determined using a one-way ANOVA with Dunnett's post-test. *D*, average resting membrane potentials in muscle cells of SLO-1(lf) and DAPC(lf) mutants do not differ from WT (mean ± S.E.; $n \geq 7$ per genotype), suggesting the SLO-1 and the DAPC is not involved in maintaining resting muscle tone.

brane repolarization through proper localization of the BK channel SLO-1. In addition, the findings highlight a novel role of SLO-1 in regulating postsynaptic muscle physiology, as previous studies in *C. elegans* have only implicated neuronal SLO-1 function in neurotransmitter release (28) and behavioral sensitivity to ethanol (33). Several studies have demonstrated the presence of BK channels in mammalian skeletal muscle cells, including human, although the mechanism by which they regulate muscle excitability or behavior is less well understood (34–38). In vertebrate smooth muscle, BK channels have been shown to regulate membrane potential and repolarization of action potentials, and loss of BK channels enhance urinary bladder contractility and behavioral urinary incontinence (39–42). In the vertebrate CNS, in contrast, mice lacking BK channels display depolarization-induced inactivation of action potentials in cerebellar Purkinje neurons and behavioral cerebellar ataxia (43). However, the functional role of SLO-1 in the mammalian CNS may vary depending on neuronal context and

subcellular localization (44).Nonetheless, our findings more closely mirror the observed physiological function of SLO-1 in vertebrate smooth muscle cells, as we see an enhancement, not reduction, in AP frequency resulting from SLO-1(lf). This may suggest fundamental differences in cellular properties or BK channel function in neurons *versus* smooth or skeletal muscle.

The observation that DAPC mutants do not display alterations in neuronal SLO-1 localization, based on the lack of broadened EPSCs across all DAPC mutants (Fig. 1, *E* and *F*) as well as normal SLO-1::GFP expression intensities at the dorsal and ventral nerve cords (Fig. 3, *C* and *D*), further suggests that the DAPC exclusively regulates SLO-1 function postsynaptically to shape muscle excitability and behavior. Several lines of evidence from previous studies support this conclusion. For example, muscle-specific rescue of *stn-1* is sufficient to reverse aldicarb-hypersensitivity and hyperactivity of *stn-1* mutants (13). Similarly, muscle but not neuronal rescue of *dys-1*, *slo-1*, and *dyc-1* is able to suppress the head-bending phenotype in each respective mutant (14, 15, 17). Furthermore, muscle-specific expression of the SLO-1-interacting protein, ISLO-1, is sufficient to rescue the head-bending phenotype in *islo-1* mutants (20).

The DAPC Complex Does Not Regulate AChR Localization—In vertebrate studies, aberrant AChR localization and expression is observed concomitantly with muscle degeneration and/or morphological defects in NMJ structure in several DAPC-null mutants (1, 8–10, 45). It is therefore difficult to discern whether the DAPC complex directly regulates AChR architecture, or indirectly affects AChR localization through the maintenance of cytoskeletal muscle morphology. In *C. elegans*, muscle degeneration resulting from the loss of DAPC function is only observed in a sensitized *hlh-1* (homologue of human Myogenin required for proper muscle development) hypomorphic background, with DAPC and *hlh-1* single mutants showing no muscle degeneration in young adult populations (13, 14, 17, 19, 46). Experimentally, this affords the unique opportunity to address the role of the DAPC exclusively in cell signaling, independent of its role in NMJ muscle structure and morphology. Based on our findings in *C. elegans*, the DAPC complex seems to be dispensable for localization and function of AChRs at the *C. elegans* NMJ, as electrophysiological analyses revealed no alterations in evoked synaptic muscle responses in DAPC mutants. Furthermore, immunohistochemical and fluorescence analysis confirmed that disruption of the DAPC does not affect AChR distribution. As such, we propose that the DAPC does not directly regulate AChR architecture at the NMJ. It is therefore possible that alterations in AChR localization and expression at the vertebrate NMJ of DAPC mutants is a secondary consequence of muscle degeneration or structural aberration (*e.g.* morphological alteration of junctional folds), rather than evidence of a direct role of the DAPC in maintaining AChR clusters on the muscle membrane. Alternatively, it is possible that the vertebrate DAPC has appropriated an additional functional role in synaptic architecture as organisms evolved in complexity.

Implications for Muscular Dystrophy Disorders—Many studies have shown that necrosis and degeneration of dystrophic muscle is exacerbated and accelerated by muscle use. The common defect in SLO-1 muscle localization in DAPC mutants may offer an explanation for this use-dependence of muscle dystrophy or necrosis in animal models and human pathology. Current-clamp data in this study show that aberrant SLO-1 localization in DAPC mutants enhances muscle excitability during periods of prolonged synaptic stimulation, while leaving resting membrane potentials and spontaneous muscle activity unaltered (27). As such, the augmented muscle action potential firing during periods of prolonged or tetanic synaptic stimulation, due to the lack of SLO-1-mediated membrane repolarization, would consequently enhance Ca^{2+} influx through voltage-dependent calcium channels (VDCCs). Additionally, excessive mechanical strain on dystrophic muscle during contractile activity has been shown to induce micro-tears in the sarcolemmal membrane (see Ref. 47 for review), which could trigger stress-induced Ca^{2+} release from intracellular stores and further exacerbate the dysregulation of Ca^{2+} signaling. Rises in intracellular Ca^{2+} have long been linked to cellular stress and toxicity, and several studies have shown enhanced subsarcolemmal [Ca^{2+}] in dystrophic muscle (see Ref. 48 for review). Together, enhanced muscle excitability and tears in the muscle membrane, both of which occur only during strong contractile activity, may initiate a positive feed-back loop of aberrant Ca^{2+} signaling that constitutes the use-dependence of muscle degeneration. Interestingly, the VDCC EGL-19 has been shown to co-localize and functionally couple to SLO-1 in *C. elegans* body-wall muscle, and the disruption of this tight coupling between dystrophin, SLO-1, and Ca^{2+} channels in DAPC mutants is proposed to elevate intracellular Ca^{2+} concentrations that in turn facilitates muscle necrosis (20, 49). Future studies will be necessary to directly examine the consequences of SLO-1 down-regulation on Ca^{2+} signaling in DAPC mutants. Nevertheless, our study provides further evidence implicating Ca^{2+} dysregulation, due to SLO-1 mislocalization mediated muscle hyperexcitability in addition to cytoskeletal instability, in the genesis and progression of cellular pathology in muscular dystrophy diseases.

REFERENCES

1. Grady, R. M., Zhou, H., Cunningham, J. M., Henry, M. D., Campbell, K. P., and Sanes, J. R. (2000) *Neuron* **25,** 279–293
2. Willmann, R., and Fuhrer, C. (2002) *Cell Mol. Life Sci.* **59,** 1296–1316
3. Kanagawa, M., and Toda, T. (2006) *J. Hum. Genet.* **51,** 915–926
4. Meier, T., and Ruegg, M. A. (2000) *News Physiol. Sci.* **15,** 255–259
5. Carlson, C. G. (1998) *Neurobiol Dis.* **5,** 3–15
6. Pilgram, G. S., Potikanond, S., Baines, R. A., Fradkin, L. G., and Noordermeer, J. N. (2010) *Mol. Neurobiol* **41,** 1–21
7. Kong, J., and Anderson, J. E. (1999) *Brain Res.* **839,** 298–304
8. Adams, M. E., Kramarcy, N., Krall, S. P., Rossi, S. G., Rotundo, R. L., Sealock, R., and Froehner, S. C. (2000) *J. Cell Biol.* **150,** 1385–1398
9. Grady, R. M., Grange, R. W., Lau, K. S., Maimone, M. M., Nichol, M. C., Stull, J. T., and Sanes, J. R. (1999) *Nat. Cell Biol.* **1,** 215–220
10. Jacobson, C., Côté, P. D., Rossi, S. G., Rotundo, R. L., and Carbonetto, S. (2001) *J. Cell Biol.* **152,** 435–450
11. Vainzof, M., Ayub-Guerrieri, D., Onofre, P. C., Martins, P. C., Lopes, V. F., Zilberztajn, D., Maia, L. S., Sell, K., and Yamamoto, L. U. (2008) *J. Mol. Neurosci* **34,** 241–248
12. Gieseler, K., Abdel-Dayem, M., and Ségalat, L. (1999) *FEBS Lett.* **461,** 59–62
13. Grisoni, K., Gieseler, K., Mariol, M. C., Martin, E., Carre-Pierrat, M., Moulder, G., Barstead, R., and Ségalat, L. (2003) *J. Mol. Biol.* **332,**

1037–1046
14. Carre-Pierrat, M., Grisoni, K., Gieseler, K., Mariol, M. C., Martin, E., Jospin, M., Allard, B., and Ségalat, L. (2006) *J. Mol. Biol.* **358,** 387–395
15. Lecroisey, C., Martin, E., Mariol, M. C., Granger, L., Schwab, Y., Labouesse, M., Ségalat, L., and Gieseler, K. (2008) *Mol. Biol. Cell* **19,** 785–796
16. Gieseler, K., Bessou, C., and Ségalat, L. (1999) *Neurogenetics* **2,** 87–90
17. Bessou, C., Giugia, J. B., Franks, C. J., Holden-Dye, L., and Ségalat, L. (1998) *Neurogenetics* **2,** 61–72
18. Grisoni, K., Martin, E., Gieseler, K., Mariol, M. C., and Ségalat, L. (2002) *Gene* **294,** 77–86
19. Gieseler, K., Mariol, M. C., Bessou, C., Migaud, M., Franks, C. J., Holden-Dye, L., and Ségalat, L. (2001) *J. Mol. Biol.* **307,** 107–117
20. Kim, H., Pierce-Shimomura, J. T., Oh, H. J., Johnson, B. E., Goodman, M. B., and McIntire, S. L. (2009) *PLoS Genet.* **5,** e1000780
21. Liewald, J. F., Brauner, M., Stephens, G. J., Bouhours, M., Schultheis, C., Zhen, M., and Gottschalk, A. (2008) *Nat. Methods* **5,** 895–902
22. Frøkjaer-Jensen, C., Davis, M. W., Hopkins, C. E., Newman, B. J., Thummel, J. M., Olesen, S. P., Grunnet, M., and Jorgensen, E. M. (2008) *Nat. Genet.* **40,** 1375–1383
23. Abraham, L. S., Oh, H. J., Sancar, F., Richmond, J. E., and Kim, H. (2010) *PLoS Genet.* **6,** e1001077
24. Gendrel, M., Rapti, G., Richmond, J. E., and Bessereau, J. L. (2009) *Nature* **461,** 992–996
25. Duerr, J. S., Frisby, D. L., Gaskin, J., Duke, A., Asermely, K., Huddleston, D., Eiden, L. E., and Rand, J. B. (1999) *J. Neurosci* **19,** 72–84
26. Richmond, J. *Synaptic function* (December 7, 2007) WormBook, ed. The *C. elegans* Research Community, *WormBook*, doi/10.1895/wormbook.1.69.1, http://www.wormbook.org
27. Gao, S., and Zhen, M. (2011) *Proc. Natl. Acad. Sci. U.S.A.* **108,** 2557–2562
28. Wang, Z. W., Saifee, O., Nonet, M. L., and Salkoff, L. (2001) *Neuron* **32,** 867–881
29. Richmond, J. E., and Jorgensen, E. M. (1999) *Nat. Neurosci* **2,** 791–797
30. Touroutine, D., Fox, R. M., Von Stetina, S. E., Burdina, A., Miller, D. M., 3rd, and Richmond, J. E. (2005) *J. Biol. Chem.* **280,** 27013–27021
31. Kim, H., Rogers, M. J., Richmond, J. E., and McIntire, S. L. (2004) *Nature* **430,** 891–896
32. Liu, P., Ge, Q., Chen, B., Salkoff, L., Kotlikoff, M. I., and Wang, Z. W. (2011) *J. Physiol.* **589,** 101–117
33. Davies, A. G., Pierce-Shimomura, J. T., Kim, H., VanHoven, M. K., Thiele, T. R., Bonci, A., Bargmann, C. I., and McIntire, S. L. (2003) *Cell* **115,** 655–666
34. Nimigean, C. M., and Magleby, K. L. (1999) *J. Gen. Physiol.* **113,** 425–440
35. Bingham, J. P., Bian, S., Tan, Z. Y., Takacs, Z., and Moczydlowski, E. (2006) *Bioconjug. Chem.* **17,** 689–699
36. Tricarico, D., Mele, A., and Conte Camerino, D. (2005) *Neurobiol Dis.* **20,** 296–302
37. Wang, Y. J., Lin, M. W., Lin, A. A., and Wu, S. N. (2008) *Life Sci.* **82,** 11–20
38. McManus, O. B., and Magleby, K. L. (1991) *J. Physiol.* **443,** 739–777
39. Meredith, A. L., Thorneloe, K. S., Werner, M. E., Nelson, M. T., and Aldrich, R. W. (2004) *J. Biol. Chem.* **279,** 36746–36752
40. Hashitani, H., and Brading, A. F. (2003) *Br. J. Pharmacol.* **140,** 159–169
41. Herrera, G. M., and Nelson, M. T. (2002) *J. Physiol.* **541,** 483–492
42. Heppner, T. J., Bonev, A. D., and Nelson, M. T. (1997) *Am. J. Physiol.* **273,** C110–C117
43. Sausbier, M., Hu, H., Arntz, C., Feil, S., Kamm, S., Adelsberger, H., Sausbier, U., Sailer, C. A., Feil, R., Hofmann, F., Korth, M., Shipston, M. J., Knaus, H. G., Wolfer, D. P., Pedroarena, C. M., Storm, J. F., and Ruth, P. (2004) *Proc. Natl. Acad. Sci. U.S.A.* **101,** 9474–9478
44. Hu, H., Shao, L. R., Chavoshy, S., Gu, N., Trieb, M., Behrens, R., Laake, P., Pongs, O., Knaus, H. G., Ottersen, O. P., and Storm, J. F. (2001) *J. Neurosci.* **21,** 9585–9597
45. Côté, P. D., Moukhles, H., Lindenbaum, M., and Carbonetto, S. (1999) *Nat. Genet.* **23,** 338–342
46. Gieseler, K., Grisoni, K., and Ségalat, L. (2000) *Curr. Biol.* **10,** 1092–1097
47. Allen, D. G., Whitehead, N. P., and Yeung, E. W. (2005) *J. Physiol.* **567,** 723–735
48. Hopf, F. W., Turner, P. R., and Steinhardt, R. A. (2007) *Subcell Biochem.* **45,** 429–464
49. Alderton, J. M., and Steinhardt, R. A. (2000) *J. Biol. Chem.* **275,** 9452–9460